SUPER RESOLUTION OF TIME-LAPSE SEISMIC IMAGES

Sergio E. Zarantonello[1,2], Bonnie Smithson[3], Youli Quan[4]

[1]Algorithmica LLC (sergio@rithmica.com)
[2]Department of Applied Mathematics, Santa Clara University (szarantonello@scu.edu)
[3]Department of Electrical Engineering, Santa Clara University (bsmithson@scu.edu)
[4]School of Earth Sciences, Stanford University (quany@stanford.edu)

Abstract

We present results of an on-going project to assess the applicability in reflection seismology of emerging super resolution techniques pioneered in digital photography. Our approach involves: (1) construction of a forward model connecting low resolution seismic images to high resolution ones, and (2) solution of a *Tikhonov-regularized* ill conditioned optimization problem to construct a high resolution image from several lower resolution counterparts; the high and low resolution images derived, respectively, from dense and sparse seismic surveys.

Keywords: cloud computing, compressed sensing, reflection seismology, reverse time migration, seismic image, seismic survey, shot gather, super-resolution

1. Introduction

Seismic imaging is a technology for building images of the Earth's subsurface based on the propagation of artificially created seismic waves - explosions or mechanically-generated vibrations - that penetrate the Earth, reflect at discontinuities, and travel back to the surface where they are recorded by arrays of sensors. The construction of accurate 3-D images of the Earth's subsurface is extremely computationally and data intensive, requiring dense seismic surveys, data volumes in the order of 10-15 terabytes, and 3-D parallel applications running on thousands of processors. This cost is compounded in 4-D seismic imaging, where a sequence of time-lapse seismic images is required to monitor a time-evolving process below the Earth's surface.

In this article we outline a novel, cost-effective, 4-D procedure based on *reverse time migration* [3], an advanced application for building high-quality seismic images. We do not attempt to image below the diffraction limit. Our procedure relies on a much smaller than normally required set of *shot-gathers*, *i.e.* seismic sources and associated sensors, and is thus much less expensive than conventional 4-D monitoring with dense surveys. Furthermore, it can improve the resolution of seismic images by incorporating what would be the effects of added sources. We interpret a sparse collection of *shot-gather images* as observation points, and apply a *compressed sensing* [5, 6, 8] methodology to recreate the seismic image that would have been obtained with a full set of shot-gathers. The procedure presents the advantage of requiring fewer sources, considerably lower operational costs, less data, and significantly less processing. In a continuing project the relevant algorithms will be implemented on *graphical processing units* (GPUs) with expected improvements in price/performance.

To assess our procedure we used a 3-D geologic model consisting of a shallow coal layer below the Earth's surface with corresponding overburden and underburden. We modeled the injection and sequestration of CO_2 in the coal layer, and simulated 4-D seismic monitoring of this process with both, dense and sparse seismic surveys. The objectives were:

1. To detect with seismic images the leakage of CO_2 to an overlaying sand unit.

2. Using the sparse survey data, to reconstruct the high resolution images obtained with the dense survey.

The organization of our paper is as follows. In Section 2 we give a brief description of the reverse time migration algorithm. In Section 3 we give an overview of the compressed sensing methodology. In Section 4 we describe the synthetic model used for evaluation and describe our procedure. In Section 5 we present results. Finally, in Section 6 we comment on the computational challenges we faced, and on our use of cloud computing in this project.

2. Reverse Time Migration.

Reverse time migration (RTM) is an advanced but computationally expensive seismic imaging technology that has spurred much interest in recent years due to: (1) its ability to image complex subsurface targets accurately, and (2) the performance improvements in computer hardware that have enabled its routine use in industry. In RTM the two-way wave equation is solved for both the source and receiver wave fields. This is followed by point-by-point multiplications of the receiver and source wave-fields (*i.e.*, zero-lag cross-correlations) which are summed over time and over shot gathers. By far the most computationally intensive part of RTM is the solution of the wave equation. In our implementation of RTM, we used an explicit finite-difference solver for the 3-D wave equation in a heterogeneous medium. The algorithm is 2nd order accurate in time and 8th order accurate in the spatial variables. Appropriate initial conditions for shot and receiver waves were given, and absorbing boundaries specified. The key aspects of RTM relevant to this paper are: (1) the high quality of the resulting seismic images and (2) the characteristics of its computational flow, which involves calculating each 3-D *shot-gather image* (the image volumes obtained by processing each separate shot-gather), and then stacking the shot-gather images to build the desired 3-D image volume.
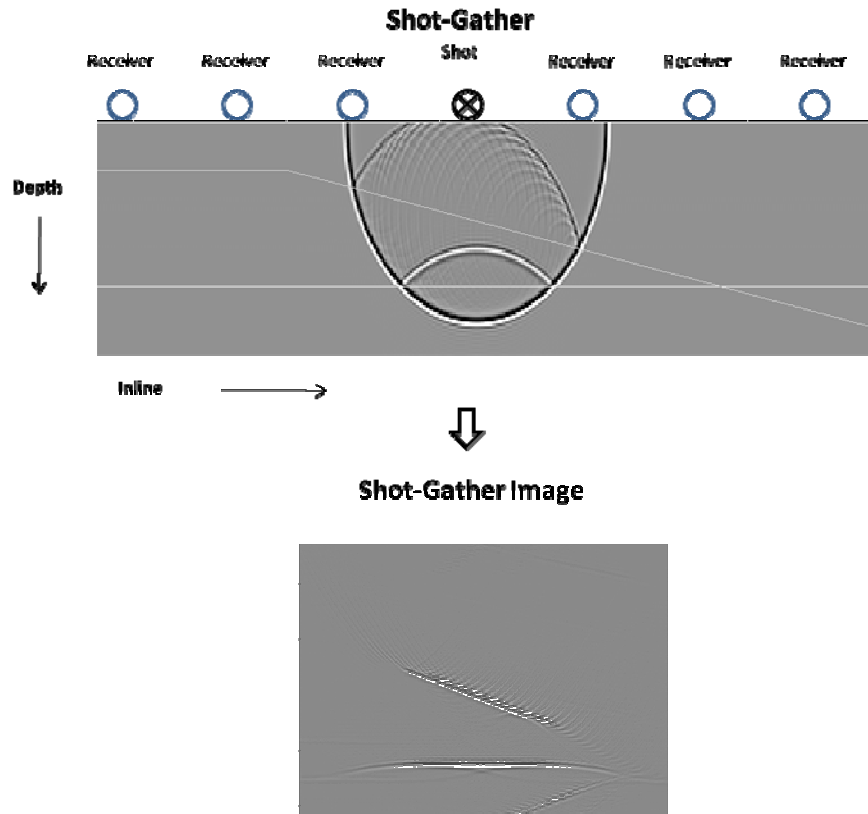
Figure 1. **Cross-section schematic of a shot-gather (above) and resulting seismic image (below). For each source location, there is a corresponding shot-gather and resulting 3-D shot-gather image. The sum of all shot-gather images gives the desired image volume.**

The RTM algorithm parallelizes at three levels: (1) shot-receiver pairs handled in a data-parallel fashion, (2) overlapped domain-decomposition in the physical domain, and (3) vector-parallel calculations of the Laplacian, source terms, and

time-updates. For a GPU adaptation, the vector-parallel calculations are blocked, pipelined, and arranged in a data-streaming mode. A complete GPU implementation of RTM scales, and delivers order-of-magnitude improvement in price/performance over conventional implementations on traditional hardware [14].
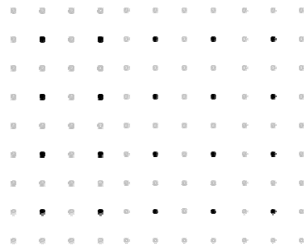

Figure 2a "Survey Domain", *i.e.* **positions of receivers and sources ("shots") on Earth's surface**
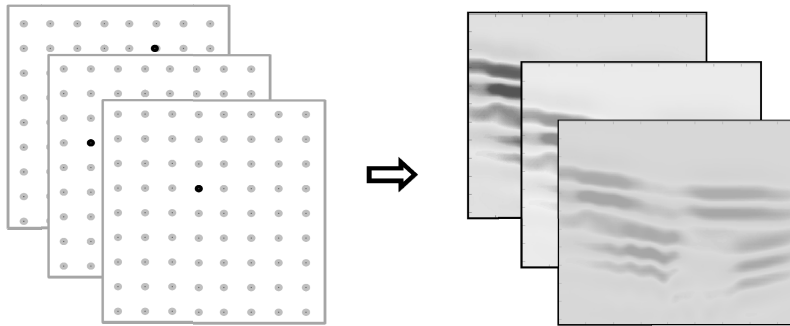

Figure 2b Shot-gathers (left), and cross-section view of corresponding 3-D shot-gather image volumes (right)
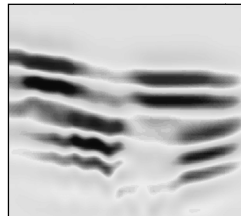

Figure 2c. Cross-section view of "stacked" 3-D image volume

In [7] Cao *et al* demonstrated the super-resolution and super-stacking properties of RTM when the velocity model is known exactly. Their tests with synthetic data showed that under these circumstances RTM has the potential of exceeding the Rayleigh resolution limit significantly, with an enhancement of the signal by a factor proportional to $N^{1/2}$ where N is the number of shot gathers. By using compressed sensing it is thereby possible to increase the resolution of seismic images by recreating virtual shot-gather images and incorporating them in the stacking process.

3. Compressed Sensing

Compressed sensing is a fundamental new technology developed by Donoho [8] and Candes *et al* [5, 6]. The basic idea is as follows: Assume an image, given as an N-dimensional vector **m**, can be represented sparsely as a linear combination of functions in a possibly redundant basis. Let **x** be the vector of coefficients of **m** in this basis, and let **T** be the corresponding transformation matrix:

$$\mathbf{m} = \mathbf{T}\,\mathbf{x} \tag{1}$$

Sampling the image involves a selection or projection matrix **P** of rank K<<N. Given a K-dimensional vector **y = P m** of samples of **m**, the objective is to reconstruct the image **m** from the samples **y.** The approach in compressed sensing is to seek the sparsest vector **x** such that

$$\mathbf{y = P\ T\ x} \tag{2}$$

Once **x** is found, the reconstructed image **m** is obtained from **m = T x**.

Since K<<N, the matrix **A = P T** is rectangular with many more rows than columns, and equation (2) is an undetermined system of equations with infinite possible solutions. The approach for finding **x** involves a nonlinear regularization of (2). The usual procedure is to find a solution **x** that among all others has the minimum L^1 norm. The premise being (and mathematically proved under certain conditions [5, 6, 8]) that the solution **x** of minimum L^1 norm has the fewest nonzero components. Zhang in [22] has a brief discussion on necessary conditions for the successful recovery of missing data *y*, and remarked that the proper selection of the matrix **T** is the key issue. In this regard, prior knowledge of the data is essential. The wavelet, curvelet, and discrete cosine (DCT) transforms are some of the generic transforms commonly used for **T**.

An alternative to finding the minimum L^1 norm solution is the Tikhonov regularization:

$$\mathbf{x:}\ \min\left(\ \|A\ \mathbf{u} - \mathbf{y}\|_2 + \gamma\ \|\mathbf{u}\|_1\ \right)\quad \mathbf{u}\ \text{in}\ R^N \tag{3}$$

where γ is a regularization parameter, and **x** is a solution to the minimization problem. In the present paper, we modify and extend the procedure of equation (3) to higher dimensions, interpreting **m** as a 2-D array of 3-D shot-gather images, and the set **y** of *observation points* as a sub-array of **m**. An outline of our approach is given at the end of Section 4.

4. Case Study

The injection, adsorption, and storage of CO_2 in coal beds has been considered as a strategy to reduce CO_2 industrial emissions into the atmosphere, with the production of desorbed CH_4 partially covering the operational costs [1, 16]. The acceptability of this strategy depends on the ability to detect early leakage of CO_2 to overlying geologic units, and give field crews lead time to lower the formation pressure before the gas reaches the surface. In an earlier study Zarantonello *et al* [21] investigated the effectiveness of time-lapsed seismic imaging with RTM to monitor CO_2 injection and sequestration in shallow coal beds, and to this effect developed a geologic model and a reservoir simulation model, representing the Big George coal seam in the Powder River Basin in Wyoming [9]. The Earth model is outlined in Fig. 3. It includes four water disposal wells at the corners and one CO_2 injector in the center. In Fig. 3 the coal reservoir is shown black. A thin semi-permeable shale layer and overlying sand unit are white. The overburden layers are shown in different shades of gray.
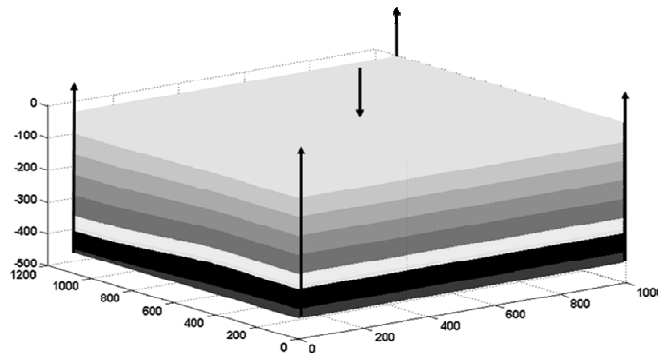

Figure 3. Earth model with CO2 injection well and water disposal wells

A dynamic reservoir simulation model of the coal and overlaying sand (derived from one built by Ross [17]) was used to model a ten-year CO_2 injection process. The CO_2 saturations and pressures predicted by the reservoir simulator, and the rock properties specified in the geologic model, were processed with rock-physics correlations [13] to construct 3-D

velocity fields at the start and end of CO2 injection. Seismic surveys were simulated, and synthetic seismic data were generated. Finally, RTM was used to build 3-D seismic image volumes representing the Earth's subsurface at the beginning and end of the ten-year CO2 injection process (year = 0 and year = 10, respectively). We used RTM because of its superior imaging capability and its ability to handle noise typical in shallow coal reservoirs. Our results showed that the CO2 plume, predicted by the reservoir simulator, was clearly detected in the seismic image volume at the end of CO2 injection (year = 10). In figure 4 shows a comparison of CO2 gas saturation, the seismic image, and acoustic velocities at the same depth below the Earth's surface.
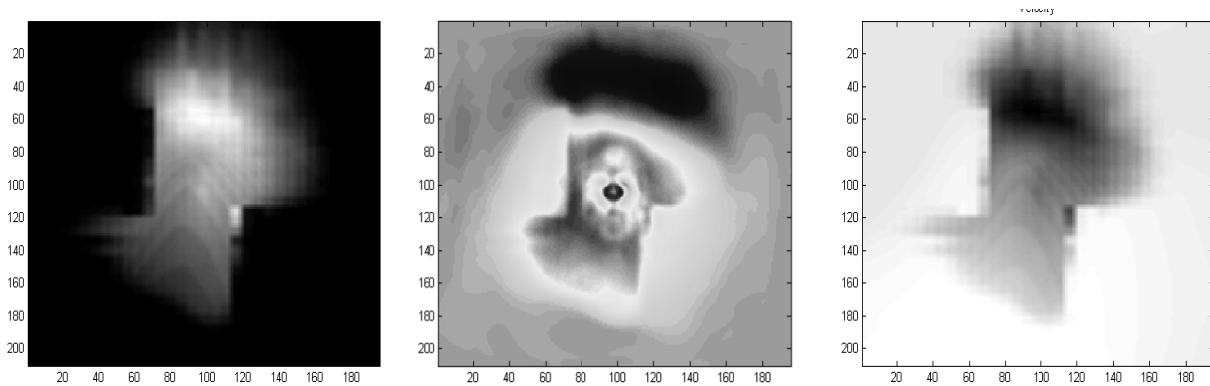
Figure 4. Depth slice of CO2 gas saturation volume (left), seismic image volume(center), and acoustic velocityvolume (right)

The purpose of our study is to show that by applying compressed sensing it is possible to obtain the same quality seismic images with sparse instead of dense seismic surveys. The idea is to consider a small subset of shot-gather images as *observation points*, and using a Tikhonov-type methodology to infer the missing shot-gather images needed to construct the high-resolution image by stacking.

In our case study, we considered a 32 x 32 (high-density) array of shot locations. We assumed the high-resolution (year = 0) baseline image volume was known, but that the year = 10 was not, except for 16 shot-gather images obtained from a regular 4 x 4 (low density) sub-array of shot locations. The shot locations for the high and low density surveys are shown in Figure 5.
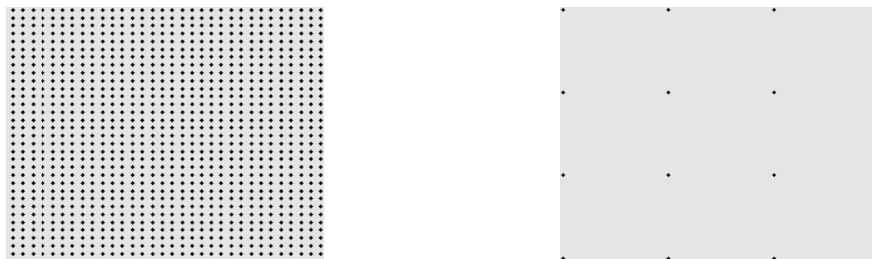
Figure 5. Areal location of shots (sources) in high and low density seismic surveys. Each shot location corresponds to a 3-D shot-gather image volume obtained with RTM. We interpreted the subset of 3-D shot-gather image volumes derived from the "small" set of source locations on the right as the *observation points*. The goal was to reconstruct the 3-D shot-gather image volumes from all shot locations on the left, and obtain the final (high-resolution) image volume by stacking.

The first step was to reconstruct the entire set of 1024 shot-gather images from the 16 available ones. This was achieved by minimizing the sum of:

1. The L^2-norm of the residual between observations and predictions.

2. A regularization parameter multiplied by the discrepancy between the L^2 norm of the prediction and its estimated value.

For proof of concept we used Daubechies D4 wavelets which gave sparse representations of the baseline image data and we deemed adequate for our purpose. [A *learned dictionary*, by optimally adapting itself to the features of the data, would appear a better choice of *basis functions,* and will be considered in future work.]

Our objective was to reconstruct the high-resolution image volume at year = 10. To each point **p** in the image volume we associated the array of contributions to its amplitude from all 32 x 32 = 1024 shots in the dense survey. These contributions constituted a 32 by 32 array we call the *image-point gather* of **p**. The *image-point gathers* of each points **p** in the image domain were presumed unknown except for the 4 by 4 sub-grid of contributions from the observations (given 16 shot-gather images). Our goal was to reconstruct the 32 by 32 *image-point gather* of each point in the image volume. Once an image-point gather was reconstructed, the sum of its array values gave the amplitude of the corresponding point ("voxel") in the high-resolution image volume.

We proceeded as follows. From an analysis of the high-density survey at year = 0, where we knew all *image-point gathers*, we found the indices of the few dominant wavelet coefficients of each. These indices determined how each point in the geologic structure was imaged as the shot location varied. Since the geologic structure was time invariant, we assumed the indices of the dominant wavelet coefficients of each *image-point gather* to be the same in year 0 as in year 10 (although their amplitudes would change as the injected CO2 accumulated below geologic layers). The problem of reconstructing the *image-point gathers* thus became that of finding the amplitudes of their relatively few dominant wavelet coefficients. This we accomplish by solving, for each point in the image volume, the optimization problem

$$\mathbf{x:} \quad \min_{\mathbf{u}} \left(\|A\,\mathbf{u} - \mathbf{y}\|_2 + \gamma \, | \|\mathbf{u}\|_2 - E_{est}| \right), \quad \mathbf{u=[u_d;0]} \text{ in } R^N , \qquad \qquad \textbf{(4)}$$

where E_{est} was the estimated L^2 norm of the sought *image-point gather (*an additional piece of information), γ was a regularization parameter, $\mathbf{u}_d$ the vector of dominant two-dimensional D4 wavelet coefficients of the *image-point gather*, and **0** the remaining zero-amplitude coefficients. Once the solution of (4) was found, we took an inverse two-dimensional D4 wavelet transform, added the array values, and aggregately imaged each point in the desired high-resolution volume.

5. Results and Conclusions

In Figure 6, we show a particular 32 x 32 *image-point gather* (for a "pixel" of coordinates x = 100, y= 100) derived from a dense set of shot-gathers. By solving Equation 4 and taking an inverse 2-D wavelet (D4) transform, we reconstructed an approximation using observation values on a 4 x 4 sub-grid. The left panel shows the 32 x 32 *image-point gather* obtained with the full set of shot-gathers. The right panel shows the observation points used to reconstruct the particular *image-point gather*. In Figure 7, on the right panel we show the location of its dominant wavelet coefficients (derived from the baseline year = 0 survey), and on the left the *image-point gather* that was reconstructed with the 16 observations. In Figure 8, we compare the same depth slice of three 3-D seismic image volumes: (a) using 1024 shot gathers with shot locations on a 32 x 32 grid, (b) using 16 shot gathers with shot locations on a 4 x 4 sub-grid, and (c) our final result, the super-resolved depth slice constructed with 16 shot gathers.

For compressed sensing to be successful, the normally acquired data must be redundant in terms of its *information content*. Under such circumstances it is sufficient to acquire a smaller (in many cases much smaller) data set. This appears to be the case with seismic data. Our work suggests that a significant cost reduction in field operations is possible since the number of shot-gathers dominates the cost of a land survey, and this number can be reduced significantly without loss of quality in the *reconstructed* seismic images. Alternatively, applying a compressed sensing to image data from a seismic survey, it is possible to construct the (super-resolved) seismic images that would have been obtained with a much denser survey. The results and procedures presented are part of an on-going effort to apply

compressed sensing and super-resolution techniques in reflection seismology. We are encouraged by the results obtained so far, and believe these will be improved significantly in our continuing work.
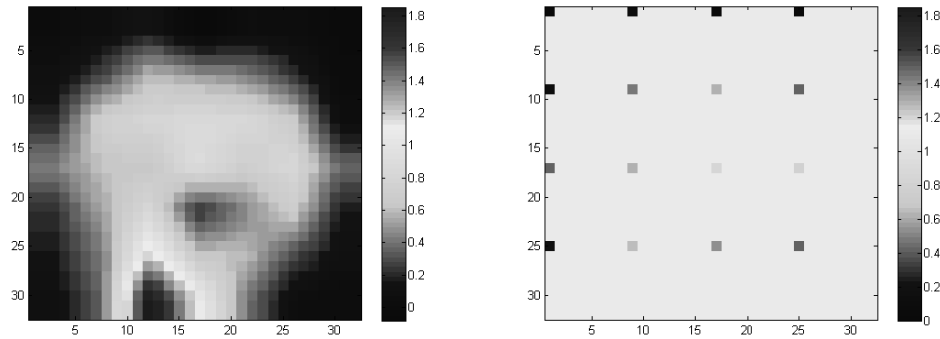

Figure 6. 32 x 32 *image-point gather* derived from dense survey (left). 4 x 4 subgrid of observations (right)
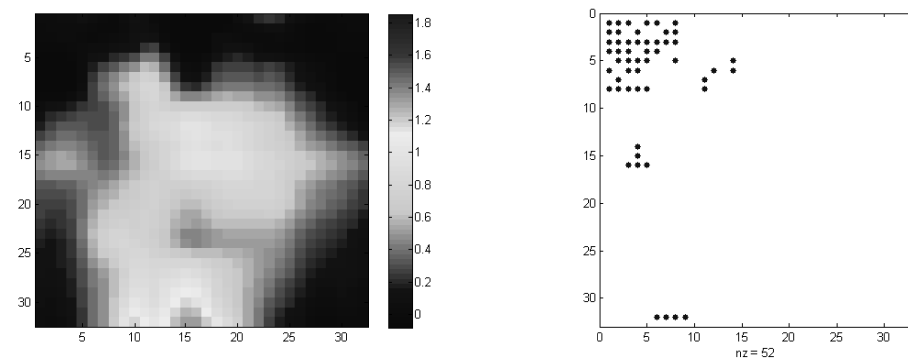

Figure 7. Reconstructed *image-point gather* (left) built with the 16 observations of Figure 6. Incidence matrix of 2-D D4 wavelet transform (right) showing the dominant coefficients in the wavelet domain.
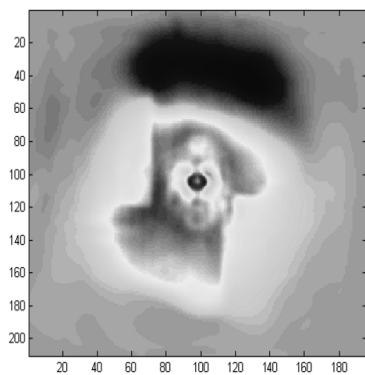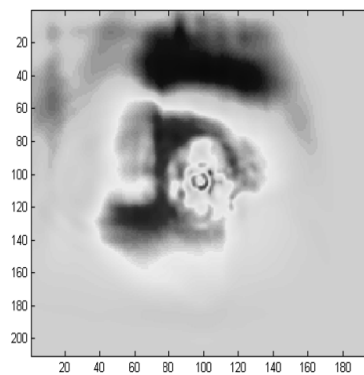

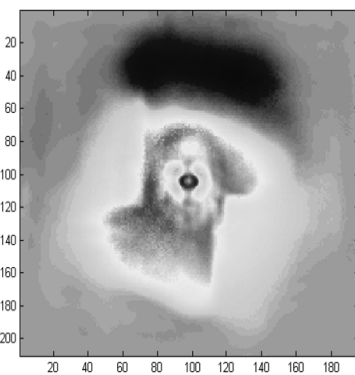**Figure 8a. "HR" image**   **Figure 8b. "LR" image**   **Figure 8c. Reconstructed image**

6. Computational Environment

Our project was computationally intensive, and having the necessary computer resources to complete it became an important issue. The initial plan was to parallelize the applications code and use GPUs.   We assessed three scenarios:

(1) Jacket from AccelerEyes, (2) Parallel Toolbox from MathWorks, and (3), a C++ solution using NVidia's NsightParallel IDE. A major drawback was that none of these options offered the flexibility of Matlab to easily develop and modify code. It also seemed too early in our research to justify the effort required in a GPU implementation. Another drawback was that we did not have one standard GPU platform, but a variety of systems with inconsistencies in terms of the type and number of processors, the operating system, and the availability of tools and libraries.

This prompted us to explore the possibilities of *cloud computing* through Amazon Web Services (AWS), with Octave as a cost-efficient alternative to Matlab. We selected Ubuntu Linux because of it is stability and good support of Octave, and during off-hours ran 40,950 compressed sensing jobs required in the example of Section 6 (to recreate all *image-point gathers* needed for a depth slice of dimensions 210 x 195). With 500 *instances* (machines in the cloud) we completed all jobs in about 4 hours. The availability of a very large number of computers, just and only when needed and at a very low cost, was a fundamental research-enabling tool. Cloud computing facilitated our work, allowing an efficiency not possible with traditional venues. Learning and effectively using cloud computing was an unanticipated but valuable part of our project.

References

[1] **Agrawal, A**., (2003), *The economic feasibility of enhanced coalbed methane recovery using CO2 sequestration in the San Juan Basin*, Texas A&M University, Thesis.

[2] **Arogunmati, A. and J., Harris**, (2010), *A data-estimation based approach for quasi-continuous reservoir monitoring using sparse surface seismic data*, 72nd EAGE Conference & Exhibition, Extended Abstracts.

[3] **Baysal, E., D. D. Kosloff, and J. W. C. Sherwood**, (1983), *Reverse time migration*, Geophysics, 48, no. 11, 1514-1524.

[4] **Bevc, D., Donoho, D. L., and Zarantonello, S. E**., (2004), *Application of 2nd generation wavelets in seismic imaging*, Proceedings of 74'th Ann. Internat. Mtg: Soc. of Expl. Geophys, , Extended Abstracts.

[5] **Candès E., J. Romberg, and T. Tao**. (2006), *Robust uncertainty principles: Exact signal reconstruction from highly incomplete frequency information*, IEEE Trans. Inf. Theory, **52**, No. 2, 489-509.

[6] **Candès E., and M. Wakin,** (2008), *An introduction to Compressive Sampling*, IEEE Signal Processing Magazine, 21-30.

[7] **Cao, W., Schuster, G. T., Zhan, G., Hanafy, S. M., and Boonyasiriwat**, C., (2008), *Demonstration of Super-Resolution and Super-Stacking Properties of Time Reversal Mirrors in Locating Seismic Sources,* University of Utah, Thesis,

[8] **Donoho, D.** (2006), *Compressed sensing*, IEEE Trans. Inf. Theory, **52**, No. 4, 1289-1306.

[9] **Flores, R. M.,** (2004), Coalbed methane in the Powder River Basin, Wyoming and Montana: An assessment of the Tertiary-Upper Cretaceous coalbed methane total petroleum system: U.S.Geological Survey Digital Data Series, **DDS-69-C**, chapter 2.

[10] **Kuuskraa, V. & R. Ferguson,** (2008), *Storing CO$_2$ with enhanced oil recovery*, DOE/NETL-402/1312/02-07-08.

[11] **Lustig, M., D. Donoho, and J. Pauly,** (2007), *Sparse MRI: The application of compressed sensing for rapid MR imaging*, Magnetic Resonance in Medicine, **58**, 1182–1195.

[12] **Mallat, S.,** (2008), *A wavelet tour of signal processing - The sparse way*, Third edition. Academic Press, Chapter 12.

[13] **Mavko, G., Mukerji, T., and Dvorkin, J.,** (2003), *"The Rock Physics Handbook: Tools for Seismic Analysis of Porous Media"*, Cambridge University Press.

[14] **Morton, S.,** (2009)**,** *"Seismic Imaging Experiences on GPUs",* High Performance Computing Workshop, International Meeting, Soc. of Expl. Geophys. Houston, 2009.

[15] **Nemeth, T. N., Wu, C. W., and Schuster, G. T**., (1999), *"Least-squares migration of incomplete reflection data",* Geophysics 64, 208–221.

[15] Nguyen, N., (2000), "*Numerical Techniques for Image Superresolution*". Stanford University, PhD thesis.

[16] Prusty, B.K., (2008), "*Sorption of methane and CO2 for enhanced coalbed methane recovery and carbon dioxide sequestration*", Journal of Natural Gas Chemistry, Elsevier B.V.

[17] Ross, H. (2007), "*Carbon Dioxide Sequestration and Enhanced Coalbed Methane Recovery in unmineable coalbeds of the Powder River Basin, Wyoming*", Ph.D. thesis, Stanford University.

[18] Selesnick, I., R. Van Slyke and O. Guleryuz, (2004), "*Pixel recovery via L1 minimization in the wavelet domain*", 2004 International Conference on Image Processing (ICIP), **3**, 1819-1822.

[19] Sengupta, M., G. Mavko, and T. Mukerji, (2003). "*Quantifying sub resolution saturation scales from time-lapse seismic data, a reservoir monitoring case study*", Geophysics, 68, pp 803-814.

[20] Zarantonello, S. E., and Bevc, D., (2005), "*Compression of seismic data using ridgelets*", Proceedings of 75'th Ann. Internat. Mtg: Soc. of Expl. Geophys. , Extended Abstracts.

[21] Zarantonello, S.E., Bevc, D., Harris, J.M., (2010), "*Integrated Reservoir, petrophysical, and seismic simulation of CO2 storage in coal beds*", The Leading Edge, 2010, Vol 29, No. 2, pp184-190

[22] Zhang, Y., (2006), "*When is missing data recoverable*", CAAM Technical Report TR06-15 Department of Computational and Applied Mathematics, Rice University.

_____

.